Optical properties of $Nd_{1.85}Ce_{0.15}CuO_4$

C. C. Homes* and B. P. Clayman
Department of Physics, Simon Fraser University, Burnaby, British Columbia, Canada V5A 1S6

J. L. Peng and R. L. Greene
Center for Superconductivity Research, Department of Physics and Astronomy, University of Maryland, College Park, Maryland 20742
(Received 26 March 1997)

The ab-plane reflectance of a $Nd_{1.85}Ce_{0.15}CuO_4$ single crystal ($T_c = 23$ K) has been measured from ≈ 35 to 9500 cm^{-1} at temperatures above and below T_c, and the optical properties calculated from a Kramers-Kronig analysis. A rich phonon spectrum is observed, and there are a number of c-axis infrared and Raman modes that are observed at low temperature which are believed to be activated by disorder; several of these modes show evidence for electron-phonon coupling. The normal-state optical conductivity may be described by a Drude-like component and an overdamped midinfrared component. The Drude-like component narrows rapidly; at 30 K the mean free path is estimated to be ≈ 750 Å. Below T_c the Drude carriers collapse into the condensate; the plasma frequency of the δ function is determined to be $\omega_{pS} \approx 10\,000$ cm^{-1}. The small coherence length ($\xi_0 \approx 70$ Å) places this material into the clean limit ($\xi_0/l \ll 1$). The London penetration depth is determined to be $\lambda_{ab} = 1600 \pm 100$ Å, which places it well off the Uemura line. Estimates of the electron-phonon coupling from normal-state transport measurements of $\lambda_{tr} < 0.5$, and the absence of Holstein sidebands below T_c, indicate that the carriers that participate in superconductivity are weakly coupled to the phonons. The small values for the penetration depth and the electron-phonon coupling constant suggest that the superconductivity in this material is not due to the electron-phonon mechanism, and is different than in other hole-doped superconducting cuprates. [S0163-1829(97)00434-7]

I. INTRODUCTION

In most high-temperature (high-T_c) superconducting cuprates, such as $YBa_2Cu_3O_{7-\delta}$ and $La_{2-x}Sr_xCuO_4$, the charge carriers are doped holes. However, in $Nd_{2-x}Ce_xCuO_4$, where superconductivity is induced by substituting Nd^{3+} with Ce^{4+}, the CuO_2 planes are believed to be doped with electrons[1] as well as holes.[2] Another important difference between $Nd_{2-x}Ce_xCuO_4$ and other cuprate superconductors is the coordination of the planar copper atoms.[3] In orthorhombic $YBa_2Cu_3O_{7-\delta}$ and tetragonal $La_{2-x}Sr_xCuO_4$ apical oxygen atoms sit above and below the copper atoms, yielding a nearly octahedral coordination. However, $Nd_{2-x}Ce_xCuO_4$ is a modified tetragonal (D_{4h}^{17}) structure which is composed of two-dimensional sheets of Cu-O layers with no apical oxygen atoms, resulting in copper atoms with square coordination. Within the Nd(Ce)O layers in between the CuO_2 planes, the Nd(Ce) and O atoms are not coplanar. The resistivity perpendicular to the CuO_2 planes is much higher than that in the planes ($\rho_{ab} \ll \rho_c$), and there is some evidence for an incipient metal-insulator transition along the c axis in these materials at low temperature.[4]

The $Nd_{2-x}Ce_xCuO_4$ system has attracted a great deal of interest because of its possible conventional BCS s-wave pairing in the superconducting state, as opposed to the unconventional d-wave behavior proposed for the hole-doped cuprates.[5,6] The microwave surface impedance measurements on both thin films and single crystals have shown evidence for a conventional BCS s-wave behavior with a gap of $2\Delta \approx 4k_BT_c$.[7–9] Tunneling measurements have also shown a resemblance to conventional superconductors.[10] However, the magnetic-field dependence of the specific-heat anomaly[11,12] and thin-film transmission[13] of $Nd_{2-x}Ce_xCuO_4$ both show a non-BCS-like behavior.

Whether or not this system can be considered as a conventional BCS-type superconductor is an important question, given the strong evidence that the other hole-doped cuprates are not. Infrared techniques have long been acknowledged as a powerful method for probing the electronic properties of metals and superconductors,[14,15] and may provide information about the nature of superconductivity in $Nd_{2-x}Ce_xCuO_4$. While there have been a number of reports on the infrared[13,16–22] and Raman[23–28] properties of ceramics, thin films, and single crystals of $Nd_{2-x}Ce_xCuO_4$, to date there has been no investigation of the far-infrared optical properties of single crystals.

In this paper we report on the optical properties of $Nd_{1.85}Ce_{0.15}CuO_4$ ($T_c = 23$ K) over a wide frequency range, at temperatures above and below T_c. While the optical properties cannot make an absolute determination of the nature of the gap, they show a detailed phonon spectrum and they indicate that the coupling between the carriers that become superconducting and the phonons is very small, suggesting that the pairing mechanism is not phonon mediated. The small value for the penetration depth also separates this material from other cuprate superconductors.

II. EXPERIMENT AND SAMPLE PREPARATION

Large, single crystals of $Nd_{1.85}Ce_{0.15}CuO_4$ were grown from a CuO-based flux using a directional solidification technique.[29] A mixture of high-purity (99.9%) starting materials of Nd_2O_3, CeO_2, and CuO were heated rapidly to just

 © 1997 The American Physical Society

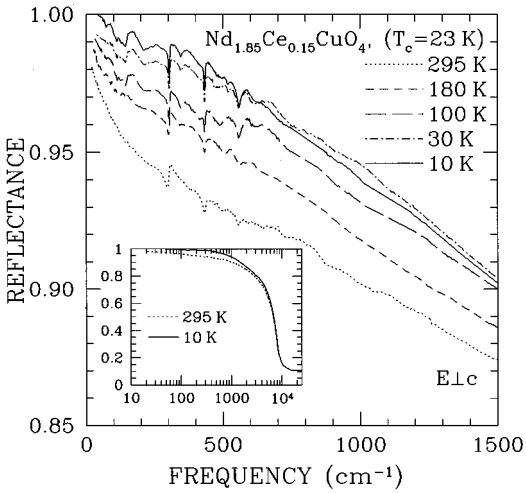

FIG. 1. The reflectance of $Nd_{1.85}Ce_{0.15}CuO_4$ (T_c=23 K) for $E\perp c(\|ab)$ at several temperatures above T_c (295, 180, 100, and 30 K), and below T_c at 10 K from ≈30 to 1500 cm^{-1}. At low temperatures, the reflectance is over 95% below ≈1000 cm^{-1}. Inset: The reflectance at 295 and 10 K over a much wider frequency range.

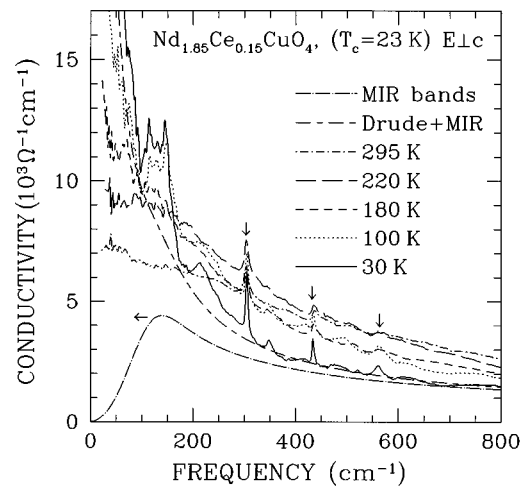

FIG. 2. The real part of the optical conductivity $\sigma_1(\omega)$ for $Nd_{1.85}Ce_{0.15}CuO_4$ (T_c=23 K) for $E\perp c$ from ≈30 to 800 cm^{-1} at several temperatures above T_c (295, 220, 180, 100, and 30 K) in the normal state. In the normal state, the conductivity may be approximated by a Drude component (dashed line) and a mid-infrared band (dash-dot line), which have been drawn for the 30 K data. The extrapolated value for σ_{dc} at 295 K is ≈7000 Ω^{-1} cm^{-1}, while at low temperature just above T_c the Drude component has narrowed considerably and $\sigma_{dc}\approx 5\times 10^4$ Ω^{-1} cm^{-1}. The downward pointing arrows denote vibrations which are present at 295 K. The arrow pointing left indicates that satisfactory fits may also be obtained using overdamped midinfrared oscillators at very low ($\omega\rightarrow 0$) frequencies.

above the melting point (1270°C for this Ce concentration). After a soak of of several hours at the maximum temperature, the materials were cooled slowly to room temperature. During the course of the growth, the flux was allowed to flow out of the crucible at the end of the growth process, so that free-standing crystals are left in the bottom of the crucible that do not need to be mechanically separated from the flux. To induce superconductivity, the crystals were annealed in an inert gas atmosphere.[29]

The reflectance of a single crystal of $Nd_{1.85}Ce_{0.15}CuO_4$ has been measured for the radiation polarized parallel to the ab plane from ≈30 to 9500 cm^{-1}, at temperatures above and below T_c on a Bruker IFS113V Fourier-transform interferometer, using a sensitive overfilling technique.[30] The crystal examined in this case was ≈2×2 mm in the ab plane, but was quite thin along the c axis (≈50 μm). The crystal had a flat, mirrorlike surface that was free of flux. Both resistivity and magnetization showed a sharp superconducting transition at 23 K, with a width of $\lesssim$1 K.[29]

The optical properties (i.e., the complex conductivity $\tilde{\sigma}=\sigma_1+i\sigma_2$) have been calculated from a Kramers-Kronig analysis of the reflectance, which requires extrapolations at high and low frequencies. At low frequency, the reflectance was extrapolated to zero frequency by assuming a Hagen-Rubens $1-R\propto\sqrt{\omega}$ dependence above T_c, and a superconducting $1-R\propto\omega^2$ dependence below T_c. The reflectance has been extended to high frequency using the data of Zhang *et al.* for $Nd_{1.80}Ce_{0.2}CuO_4$ (≈6 eV),[20] and Uchida *et al.* for La_2CuO_4 (≈35 eV),[21] above which a free-electron ($R\propto\omega^{-4}$) behavior was assumed.

III. RESULTS AND ANALYSIS

The ab plane reflectance for $Nd_{1.85}Ce_{0.15}CuO_4$ (T_c=23 K) is shown in Fig. 1 from ≈30 to 1500 cm^{-1} at several temperatures above T_c (295, 180, 100, and 30 K), and below T_c at 10 K. The inset shows the reflectance at 295 and 10 K over a much wider frequency range. The reflectance of $Nd_{1.85}Ce_{0.15}CuO_4$ displays a strong ''metallic'' character, and is over 90% for $\omega<1000$ cm^{-1} at 295 K. There is a substantial temperature dependence in the reflectance, which increases quickly with decreasing temperature until at 30 K it is over 95% in the same frequency range. The high values of the reflectance contrasts with a the lower reflectance of a similar hole-doped material $La_{1.85}Sr_{0.15}CuO_4$ material.[21] Also, the characteristic ''ledge'' in the reflectance at ≈450 cm^{-1} that is observed in many of the hole-doped cuprates[15] is absent in this material. Despite the high values for the reflectance, there is a great deal of fine structure below ≈600 cm^{-1} visible at 295 K; this structure becomes sharper as the temperature is lowered and a number of new features are observed as well.

The real part of the optical conductivity $[\sigma_1(\omega)]$ has been calculated from a Kramers-Kronig analysis of the reflectance curves in Fig. 1. The normal-state conductivity ($T>T_c$) is shown in Fig. 2 from ≈30 to 800 cm^{-1} at 295, 220, 180, 100 K, and just above T_c at 30 K. The normal-state conductivity can be described in general terms as a Lorentzian centered at zero frequency and an overdamped midinfrared component. At room temperature the conductivity associated with the zero-frequency Lorentzian is quite broad. However, as the temperature is lowered there is a rapid narrowing of this feature as spectral weight is transferred from high to low frequencies, while the conductivity at high frequency shows little change with temperature.

Figure 3 shows $\sigma_1(\omega)$ over the same frequency range just above T_c at 30 K, and below T_c at 10 K; the inset in Fig. 3

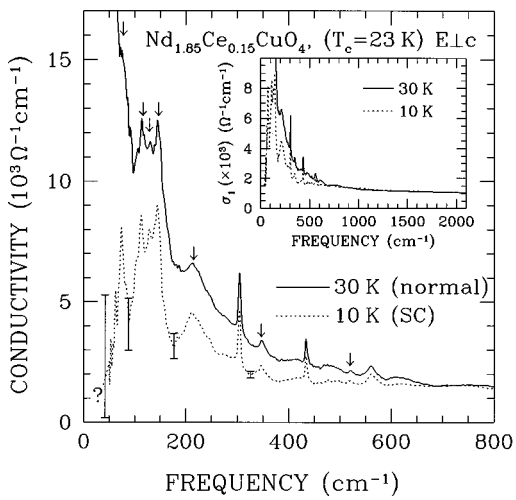

FIG. 3. The real part of the optical conductivity $\sigma_1(\omega)$ for $Nd_{1.85}Ce_{0.15}CuO_4$ ($T_c=23$ K) for $E\perp c$ just above T_c at 30 K, and below T_c at 10 K, from $\approx$30 to 800 cm^{-1}. The missing area between the two curves represents the spectral weight of the condensate. The downward pointing arrows denote spectral features that are not present in $\sigma_1(\omega)$ at 295 K. The error bars at 10 K represent the uncertainty in $\sigma_1(\omega)$ given an error of $\pm 0.1\%$ in the reflectance. Inset: The optical conductivity at 10 and 30 K over wider frequency range. There is little difference in $\sigma_1(\omega)$ for these two temperatures in the midinfrared, where the optical conductivity is flat and featureless.

shows $\sigma_1(\omega)$ at 30 K and 10 K over a wider frequency range. While the high-frequency conductivity ($\gtrsim$800 cm^{-1}) shows little temperature dependence above and below T_c, the low-frequency conductivity has decreased dramatically below T_c. The missing area between these two curves is associated with the collapse of the free carriers into the superconducting condensate. A consequence of having reflectance near unity at low frequency for $T \ll T_c$ is the increase in the uncertainty of $\sigma_1(\omega)$ in the same low-frequency region. To illustrate this point, a series of error bars have been superimposed on the conductivity at 10 K in Fig. 3 which represent the range of conductivities that result from adding or subtracting 0.1% to the reflectance at 10 K; while this has little effect at high frequencies, the increase in uncertainty at low frequency is substantial.

The sharp structure seen in the reflectance in Fig. 1 can now be seen as a series of sharp resonances in Figs. 2 and 3. As noted in the reflectance, there are some features that are present in $\sigma_1(\omega)$ at room temperature, which sharpen and become more distinct as the temperature is lowered, and are indicated by the arrows in Fig. 2. However, there are a number of features that are visible only at low temperatures ($T \lesssim 100$ K), as indicated by the arrows in Fig. 3.

The optical conductivity in the cuprate-based superconductors is usually described in terms of one-component or two-component models. In the two-component model, there are two channels of conductivity; (i) a Drude component with a temperature-dependent damping, and (ii) a broad midinfrared component that is essentially temperature independent. This is also referred to as a Drude-Lorentz model for the dielectric function

$$\tilde{\epsilon}(\omega)=\epsilon_\infty-\frac{\omega_{pD}^2}{\omega(\omega+i\Gamma_D)}+\sum_j\frac{\omega_{pj}^2}{\omega_j^2-\omega^2-i\gamma_j\omega}, \quad (1)$$

where ω_{pD} and Γ_D are the plasma frequency and damping of the Drude component, and ω_j, γ_j, and ω_{pj} are the frequency, damping, and effective plasma frequency of the jth Lorentzian contribution (phonon, interband excitation, etc.). The phonon features in the conductivity are symmetric, and have been fit using simple Lorentzian oscillators with either linear or polynomial backgrounds. The results of the phonon fits to $\sigma_1(\omega)$ at 295, 30, and 10 K are listed in Table I.

However, one of the difficulties of the two-component model is that to reproduce the broad, flat region of the conductivity in the midinfrared, several overdamped oscillators must be included as well as a Drude component. While the combination of Drude and midinfrared bands fit the conductivity at 30 K reasonably well[31] (as shown in Fig. 2), the large number of parameters and the large amount of spectral weight associated with the low-frequency midinfrared oscillators, makes it difficult to put much faith in the returned values of ω_{pD} and Γ_D.

The arbitrary nature of the midinfrared bands in the two-component model have lead to the more general assumptions of the one-component, or generalized Drude model, in which the damping rate is frequency dependent,

$$\tilde{\epsilon}(\omega)=\epsilon_\infty-\frac{\omega_p^2}{\omega[m^*(\omega)/m][\omega+i\Gamma(\omega)]}, \quad (2)$$

where ω_p is the Drude plasma frequency of the charge carriers, and $\Gamma(\omega)=1/\tau(\omega)$ and $m^*(\omega)/m$ describe the frequency-dependent (unrenormalized) carrier scattering rate and effective mass enhancement over the bare (or optical) mass. The effective mass is also given by $m^*(\omega)=m[1+\lambda(\omega)]$, where $\lambda(\omega)$ is a frequency-dependent renormalization. The complex conductivity is $\tilde{\sigma}(\omega)=-i\omega\tilde{\epsilon}(\omega)/(4\pi)$, which neglecting the contributions due to ϵ_∞, is $\tilde{\sigma}(\omega)=\omega_p^2/\{4\pi[m^*(\omega)/m][\omega-i\Gamma(\omega)]\}$. The $1/\tau(\omega)$ and $\lambda(\omega)$ can be found experimentally by

$$\frac{1}{\tau(\omega)}=\frac{\omega_p^2}{4\pi}\mathrm{Re}\left[\frac{1}{\tilde{\sigma}(\omega)}\right] \quad (3)$$

and

$$\frac{m^*(\omega)}{m}=1+\lambda(\omega)=\frac{\omega_p^2}{4\pi\omega}\mathrm{Im}\left[\frac{1}{\tilde{\sigma}(\omega)}\right]. \quad (4)$$

The plasma frequency may be determined experimentally from the optical conductivity sum rule, $I(\omega)=(120/\pi)\int_0^\omega\sigma_1(\omega')d\omega'$. (Note that this normalization is due to the fact that the optical conductivity is in units of Ω^{-1} cm^{-1}.) If the conductivity is due purely to a free-carrier response, then $I(\omega\to\infty)=\omega_p^2$. Figure 4 shows the value of this integral as a function of frequency in the normal state as well as below T_c. Regardless of whether the one- or two-component model is adopted, the low-frequency behavior is associated with the free-carrier response and the high-frequency component of $\sigma_1(\omega)$ is generally considered to be due to bound excitations which show little temperature de-

TABLE I. The fitted phonon parameters for the infrared active modes in the ab plane of $Nd_{1.85}Ce_{0.15}CuO_4$ at 295, 100, and 10 K. In Nd_2CuO_4 the four E_u and two E_g infrared modes are expected to be active in the ab plane, while the three A_{2u} infrared modes, and the A_{1g} and B_{1g} Raman modes are expected along the c axis only. The ''obs'' column refers to modes previously observed in ceramic materials. (All units are in cm^{-1}.)

		295 K			30 K			10 K		
Mode	(obs)	$\omega_{TO,i}$ ($\omega_{LO,i}$) [a]	γ_i	ω_{pi}	$\omega_{TO,i}$	γ_i	ω_{pi}	$\omega_{TO,i}$	γ_i	ω_{pi}
E_u		564.1 (596)	16.9	420	561.3	15.9	630	562.3	15.5	645
A_{2u}	(516) [c]				521.6	7.6	254	519.9	8.7	256
E_u		439.8 (506)	15.7	544	434.2	4.2	508	434.1	4.4	522
B_{1g}	(344) [b]				349.1	11.5	539	347.2	13.6	602
E_u	(304) [c]	303.2 (490)	10.2	837	304.8	4.8	855	304.3	4.7	831
A_{1g}	(225) [b]				≈220	≈30	≈1300	≈216[e]		
A_{2u}, E_u	(134) [b]				146.4	≈10	≈1500	145.0 [e]		
A_{2u}, E_u	(132) [c]				130.8	≈8	≈900	130.8 [e]		
A_{2u}, E_u					114.7	≈8	≈990	112.5 [e]		
CF [d]					78 [e]			74 [e]		

[a]The frequency of the longitudinal optic modes have been calculated from $\omega_{LO,i}^2=\omega_{TO,i}^2+\omega_{pi}^2/\epsilon_\infty$, ($\gamma_{TO,i}=\gamma_{LO,i}$) where $\epsilon_\infty=4.7$.
[b]Ref. 17 ($Nd_{1.85}Ce_{0.15}CuO_4$ ceramic at 10 K).
[c]Ref. 24 ($Nd_{1.85}Ce_{0.15}CuO_4$ ceramic at 10 K).
[d]CF refers to a possible low-lying electronic transition due to crystal-field excitations, as discussed in Ref. 28.
[e]The uncertainty in the background does not allow the widths and strengths to be reliably fitted below T_c for these modes.

pendence. In the normal state the spectral weight associated with the free carriers shifts to low frequency with decreasing temperature; this is reflected in the rapid increase in the value of the integral in Fig. 4 at low frequency. Once the integration of the free-carrier component is complete and only the temperature-independent bound excitations contribute to the integral, then the curves should converge and this value should be $\approx\omega_p^2$. As Fig. 4 illustrates, the normal-state curves have all merged by $\approx$2500 cm^{-1}, yielding a value for $\omega_p=16\,000\pm800$ cm^{-1}. The conductivity sum rule also provides a good estimate for the plasma frequency of the condensate, $\omega_{pS}^2=(120/\pi)\int_0^\infty[\sigma_{1n}(\omega)-\sigma_{1s}(\omega)]d\omega$, where $\sigma_{1n}(\omega)$ and $\sigma_{1s}(\omega)$ the are frequency-dependent conductivities for $T\approx T_c$ and $T\ll T_c$, respectively. This sum rule yields $\omega_{pS}=10\,000\pm800$ cm^{-1}. This missing spectral weight from the sum rule at 2500 cm^{-1} is indicated by two solid dots in Fig. 4 (the upper point corresponds to ω_p^2 and the lower point to $\omega_p^2-\omega_{pS}^2$). The plasma frequency of the condensate is related to the strength of the δ function by $\delta\propto\omega_{pS}^2$, and $\omega_{pS}^2=4\pi n_s e^2/m^*$, where n_s is the density of superconducting carriers, and m^* is their effective mass.

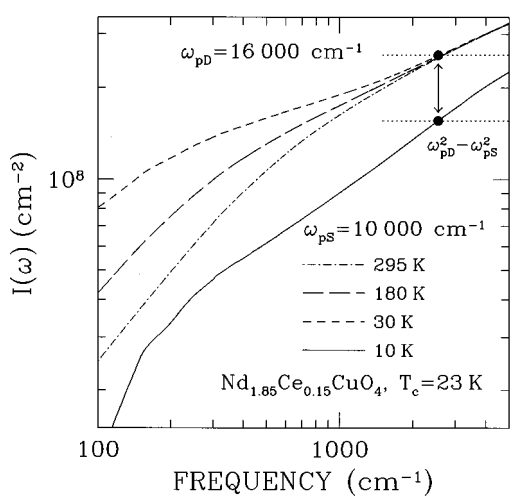

FIG. 4. The value of the conductivity sum rule integral $I(\omega)=(120/\pi)\int_0^\omega\sigma_1(\omega')d\omega'$ for $Nd_{1.85}Ce_{0.15}CuO_4$ in the infrared frequency range at 295, 180, 30, and 10 K. In the normal state, all the curves have converged by $\approx$2500 cm^{-1} indicating that the temperature-dependent free carriers have been completely integrated, yielding $\omega_p=16\,000\pm800$ cm^{-1}. Below T_c at 2500 cm^{-1} the sum rule is significantly lower; this decrease is estimated by $\omega_p^2-\omega_{pS}^2$, where $\omega_{pS}=10\,000$ cm^{-1} is the estimated plasma frequency of the condensate.

The value of $\omega_p=16\,000$ cm^{-1} is used to calculate $m^*(\omega)/m$ and $1/\tau(\omega)$, which are shown in the upper and lower panels in Fig. 5, respectively. For $T<T_c$, $\sigma_1(\omega)$ is suppressed at low frequency (as shown in Fig. 3) so that the complex conductivity will be dominated by the imaginary term $\sigma_2(\omega)=\omega_{pS}^2/(4\pi\omega)$. In this case the low-frequency mass enhancement gives the ratio of ω_p^2 to ω_{pS}^2, $1+\lambda(\omega)=\omega_p^2/\omega_{pS}^2$.[32] In Fig. 5(a), $1+\lambda(\omega\to0)\approx2.5$ at 10 K, indicating that $\approx$40% of the free carriers have condensed, in good agreement with the existing values for ω_p and ω_{pS} determined from sum rules.

The frequency-dependent penetration depth $\lambda_{ab}^{-1}(\omega)=2\pi\sqrt{\omega\sigma_2(\omega)}$ at 10 K is shown in the inset in Fig. 5(a). The extrapolated zero-frequency value is $\approx$1600 Å. The penetration depth is related to the plasma frequency of the condensate, $\lambda_{ab}^{-1}=2\pi\omega_{pS}$, so that a $\lambda_{ab}(\omega\to0)=1600$ Å yields $\omega_{pS}\approx10\,000$ cm^{-1}, again in good agreement with the sum-rule value. The fact that $\lambda_{ab}(\omega)$ shows some frequency de-

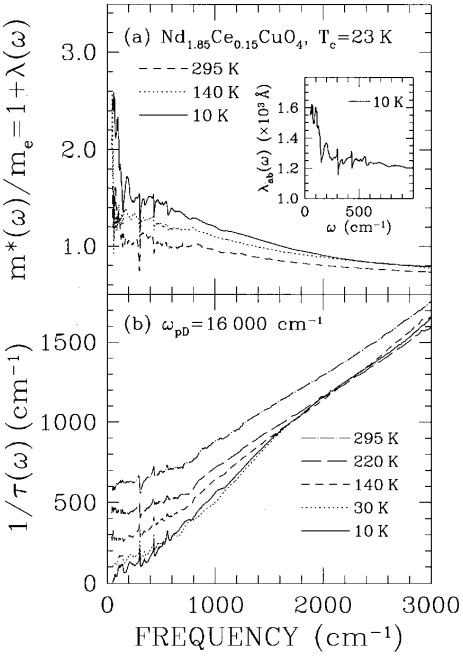

FIG. 5. (a) The frequency-dependent mass enhancement $m^*(\omega)/m=1+\lambda(\omega)$ for $Nd_{1.85}Ce_{0.15}CuO_4$ from $\omega\approx 50\ \mathrm{cm}^{-1}$ to $3000\ \mathrm{cm}^{-1}$ at 295, 140, and 10 K (using $\omega_p=16\,000\ \mathrm{cm}^{-1}$). At 10 K, $m^*(\omega\to 0)/m=\omega_p^2/\omega_{pS}^2$ is extrapolated to ≈ 2.5. This indicates that $\approx 40\%$ of the free carriers have condensed into the δ function, and gives $\omega_{pS}\approx 10\,120\ \mathrm{cm}^{-1}$. Inset: the frequency-dependent penetration depth $\lambda_{ab}^{-1}(\omega)=2\pi[\omega\sigma_2(\omega)]^{1/2}$ at 10 K [here the units of $\sigma_2(\omega)$ are in cm^{-1}]; extrapolating to zero frequency $\lambda_{ab}(\omega\to 0)\approx 1600$ Å. (b) The unrenormalized frequency-dependent scattering rate at 295, 220, 140, 30, and 10 K. While $1/\tau(\omega)$ is linear at high frequency, a ''knee'' develops at low temperature at $\approx 1500\ \mathrm{cm}^{-1}$, below which $1/\tau(\omega)$ remains linear until developing a quadratic behavior and saturating to a finite value at low frequency. The rapid suppression of $1/\tau(\omega)$ at low frequency in the normal state is similar to the ''pseudogap'' observed in other cuprates.

pendence below $\approx 300\ \mathrm{cm}^{-1}$ is an indication that not all of the free carriers have condensed into the δ function, and that there is some low-frequency residual conductivity.

The frequency-dependent scattering rate is shown in Fig. 5(b) for several temperatures above and below T_c. While $1/\tau(\omega)$ is linear at at high frequency, a ''knee'' develops at low temperature below $\approx 1500\ \mathrm{cm}^{-1}$, below which $1/\tau(\omega)$ remains linear until taking on a quadratic behavior and saturates to a finite value at low frequency. The rapid suppression of $1/\tau(\omega)$ at low frequency in the normal state is similar to the ''pseudogap'' observed in other cuprates. However, the energy scale over which this suppression occurs is quite large ($\approx 1500\ \mathrm{cm}^{-1}$), when compared to other hole-doped cuprates, which typically show a suppression only at low frequency ($\approx 500\ \mathrm{cm}^{-1}$). Fitting the temperature-dependent linear part of $1/\tau(\omega)$ ($500\ \mathrm{cm}^{-1}\lesssim\omega\lesssim 1500\ \mathrm{cm}^{-1}$) to the form $\alpha\omega+\beta$ gives $\alpha=0.39\,(0.57)$ and $\beta=482\,(-38)$ cm^{-1} at 295 K (30 K). The small value of α, and the negative intercept of β for $T\gtrsim T_c$ is similar to the behavior of some ''overdoped'' cuprates.[32] In the one-component model, $\Gamma(\omega\to 0)=\Gamma_D$, which provides a useful connection with the two-component model and allows a comparison with transport data. The temperature-dependent damping obtained in this manner is shown in Fig. 6.

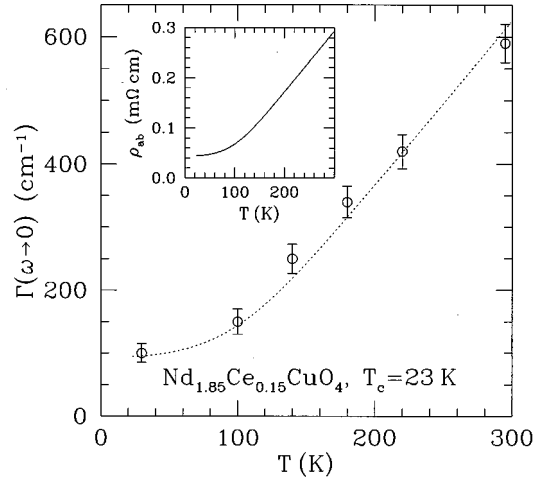

FIG. 6. The estimated value for the zero-frequency damping rate Γ_0 [$\Gamma(\omega\to 0)$] for $Nd_{1.85}Ce_{0.15}CuO_4$ in the normal state. The temperature-dependent damping has been fit (dotted line) using $\Gamma(T)=\Gamma_0+a(T-T^*)\Theta(T)+bT^2[1-\Theta(T)]$, where $\Theta(T)$ is a broadened step function (see text), and $\Gamma_0\approx 50\ \mathrm{cm}^{-1}$, $T^*=110$ K, $a=1.25\ \mathrm{cm}^{-1}\ \mathrm{K}^{-1}$, and $b=3.8\times 10^{-3}\ \mathrm{cm}^{-1}\ \mathrm{K}^{-2}$; the width of $\Theta(T)$ is about 30 K. The inset shows the estimated resistivity based on these values, which is in good agreement with transport measurements on similar crystals.

The damping varies quadratically at low temperatures, but displays a linear trend at high temperature. This behavior has been naively modeled using $\Gamma_D(T)=\Gamma_0+a(T-T^*)\Theta(T)+bT^2[1-\Theta(T)]$, where $\Theta(T)=1/\{1+\exp[(T^*-T)/\Gamma_\Theta]\}$ is a broadened step function. A good agreement with the data is obtained using $\Gamma_0\approx 100\ \mathrm{cm}^{-1}$, $a=2.6$ $\mathrm{cm}^{-1}\ \mathrm{K}^{-1}$ and $b=7.8\times 10^{-3}\ \mathrm{cm}^{-1}\ \mathrm{K}^{-2}$. The crossover temperature from quadratic to linear behavior is taken to be $T^*\approx 110$ K, and $\Gamma_\Theta=30$ K. Using these parameters and $\omega_p\approx 16\,000\ \mathrm{cm}^{-1}$, the dc resistivity may be calculated ($\rho_c=60\Gamma_0/\omega_p^2$, in units of Ω cm), and is shown in the inset in Fig. 6. A comparison of the dc resistivity deduced in this way from the optical measurements is in good qualitative agreement with transport measurements on single crystals,[29,33] in particular with regard to the linear behavior observed at high temperature. It is interesting to note that for $T<T^*$, a new phonon structure also appears, although it is uncertain if this is related to the behavior of the damping or the frequency-dependent scattering rate.

The real part of the dielectric function at several temperatures above and below T_c is shown below $1000\ \mathrm{cm}^{-1}$ in Fig. 7. The rapid decrease of $\epsilon_1(\omega)$ at low frequency with decreasing temperature is an indication of the suppression of the quasiparticle scattering rate. In a purely Drude system, the zero crossing corresponds to the location of the screened plasma frequency, $\tilde{\omega}_p^2=\omega_p^2/\epsilon_\infty$. The observed zero crossing at $\approx 8600\ \mathrm{cm}^{-1}$ would require that $\epsilon_\infty=3.5$. However, the presence of a number of excitations in the midinfrared will tend to shift the zero crossing to a higher frequency, leading to an underestimate of ϵ_∞. As a result, a value of $\epsilon_\infty=4.7$ has been determined by fitting the reflectance at high frequency.[22,23] In a system where all of the normal-state carriers collapse into the superconducting δ function, then the real part of the dielectric function in Eq. (1) becomes

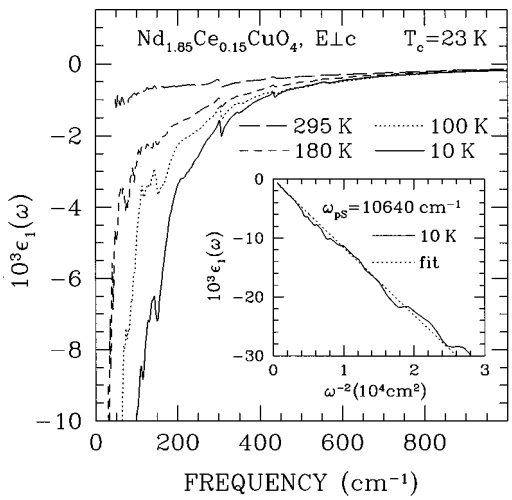

FIG. 7. The real part of the dielectric function $\epsilon_1(\omega)$ for $Nd_{1.85}Ce_{0.15}CuO_4$ ($T_c=23$ K) for $E\perp c$ at 295, 180, 100 K, and below T_c at 10 K from ≈ 35 to 1000 cm^{-1}. Inset: a plot of $\epsilon_1(\omega)$ vs ω^{-2} from $\approx 50-500$ cm^{-1}. In the clean-limit case, the slope is ω_{pS}^2, which from a linear regression is $\omega_{pS}=10\,640\pm 600$ cm^{-1}.

$\epsilon(\omega)=\epsilon'_\infty-\omega_{pS}^2/\omega^2$, where ω_{pS} is the plasma frequency of the condensate. The inset in Fig. 7 shows $\epsilon_1(\omega)$ vs ω^{-2}; a linear regression of the straight line yields $\omega_{pS}=10\,640\pm 600$ cm^{-1}, which is only slightly larger than the sum-rule value.

IV. DISCUSSION

A. Phonon spectrum

The undoped parent material Nd_2CuO_4 has a modified tetrahedral structure[3] in which a total of seven infrared-active modes are expected; three A_{2u} modes along the c axis, and four E_u modes in the ab plane. In Nd_2CuO_4, the ab-plane vibrations are observed at 130, 314, 352, and 514 cm^{-1}.[22–24] However, in Fig. 2 there are only three phonons at ≈ 303, 440, and 564 cm^{-1} present at room temperature in the ab-plane conductivity of $Nd_{1.85}Ce_{0.15}CuO_4$. It is reasonable to assume that the three strongest vibrations observed at room temperature are the E_u modes, and they have been assigned as such. This assignment of the E_u modes is in disagreement with other single-crystal work,[20,22–24] which usually assign the vibrations at ≈ 350 cm^{-1} and ≈ 520 cm^{-1} as E_u modes. However, as the results are usually quoted only at low temperature (≈ 10 K), no mention is made as to whether or not these modes are visible at room temperature. There is agreement in the literature that the strongest mode at 304 cm^{-1} is the E_u mode associated with the in-plane Cu-O bond-bending mode, while the next two E_u modes, in ascending order, are the Nd-O bond-bending and the Cu-O stretching modes.

The substitution of Ce^{4+} for Nd^{3+} in Nd_2CuO_4 not only dopes the material with electrons (holes), but it also destroys the inversion symmetry in the unit cell. This broken symmetry results in the mixing of the infrared and Raman modes, and as a result the Raman modes may become infrared active. As well, the general reduction of symmetry may also result in more general selection rules, so that vibrations in the undoped material which are active only along one polarization may become active in several in the doped material. In this way, infrared-active A_{2u} c-axis modes may appear in the ab plane. A total of four Raman-active modes are expected; the A_{1g} and B_{1g} modes are active along the c axis, while the two E_g modes are active in the ab plane. By considering that c-axis modes may be active in the ab plane, many of the assignments that we make are similar to some previous assignments made in ceramics.[16]

In previous studies[23–25] at 30 K the B_{1g} and A_{2u} modes have been observed at 344 cm^{-1} and 516 cm^{-1}, respectively. These frequencies are quite close to the two features that are activated at low temperature at 349 and 521 cm^{-1}, and strongly suggests that these two modes are the c-axis B_{1g} and A_{2u} modes, activated by disorder. Indeed, both the B_{1g} and A_{2u} modes involve the Nd(Ce)-O bonds.[24]

The A_{1g} mode is observed in Nd_2CuO_4 at 228 cm^{-1}.[23,24] Although the A_{1g} mode involves displacements of the Nd atoms, this mode has been observed in the same location in a variety of $Nd_{2-x}M_xCuO_4$ (M=Ce, Th, and Sr) materials,[23] despite the different masses of the dopant ions. This suggests that the broad feature at ≈ 220 cm^{-1} may be the A_{1g} mode. While the A_{1g} mode, which like the B_{1g} and A_{2u} modes, involves the Nd(Ce)-O bonds, may be activated by disorder, it appears to be quite strong in Figs. 2 and 3 (see Table I). Typically, modes activated by disorder are expected to be weak. It may be possible that the oscillator strength of the A_{1g} mode is enhanced by coupling to a charge-transfer mechanism. The $Nd_{2-x}Ce_xCuO_4$ materials are strongly anisotropic, and there is some evidence to suggest that the behavior along the c axis may be insulating at low temperatures.[4] It may be the case that the Nd(Ce)O planes are isolated, and that charge segregation occurs within the Nd(Ce)O planes. Typically, the charge associated with an atomic cluster is very sensitive to the configuration, or bond lengths. The effective charge is an important quantity when discussing the bonding ionicity. However, the evaluation of the effective charge is difficult for more than two kinds of atoms. For a ternary compound the extended effective charge Z_k is defined as[34]

$$\sum_i [\omega_{\mathrm{LO},i}^2-\omega_{\mathrm{TO},i}^2]=\frac{1}{\epsilon_\infty}\sum_i \omega_{pi}^2=\frac{4\pi}{V_c}\sum_k \frac{(Z_k e)^2}{M_k}, \quad (5)$$

where $\Sigma_k Z_k=0$; j denotes the phonon mode, V_c is the unit-cell volume, and k is the sum over all atoms with mass M_k and effective average charge $Z_k e$, and ω_{pi} is the effective plasma frequency of the ith phonon. In $Nd_{1.85}Ce_{0.15}CuO_4$ the constituent elements are all much heavier than the oxygen mass (M_O), so the right-hand side of Eq. (5) may be approximated by $16\pi(Z_O e)^2/(V_c M_O)$. At 295 K the oxygen effective charge is $Z_O=-1.3$, which is similar to the values of Z_O in the hole-doped cuprates[35] where $|Z_O|\approx 1-1.3$. However, below 100 K a number of new phonon features are observed, as indicated in Fig. 3. Because the oscillator strengths of the phonons below ≈ 300 cm^{-1} cannot be unambiguously determined, only the phonons above 300 cm^{-1} have been considered; this treatment gives $Z_O\approx -2$, which is the full valence for the oxygen atom in this system and indicates a substantial increase at low temperature in the average oxygen bonding. Because there is no shift in any of

the Cu-O vibrations associated with the CuO_2 planes, this suggests that there is a large degree of ionicity in the Nd(Ce)O planes. If the A_{1g} mode in neighboring unit cells are π out of phase, then the change in the local charge density may create a local dipole moment in the ab plane that is modulated at the same frequency as the A_{1g} mode, leading to enhanced oscillator strengths. This is also an alternate mechanism (that does not depend on disorder) by which c-axis vibrations may become active in the ab plane. This mechanism has also been proposed to explain the activity of the A_g modes in lightly doped $La_{2-x}Sr_xCuO_4$,[36] and is commonly observed in quasi-one-dimensional molecular crystals where the totally symmetric modes are not only observed in directions transverse to their polarization but also display greatly enhanced oscillator strengths due to this charge-transfer mechanism.[37,38]

The low-frequency conductivity is dominated by the appearance of four strong vibrations at $\approx$78, 118, 129, and 147 cm^{-1} (the mode at 78 cm^{-1} is visible most clearly below T_c). Both the A_{2u} c axis and E_u in-plane mode are observed at $\approx$130 cm^{-1}.[24] The E_u mode is doubly degenerate; in the presence of a symmetry-breaking process such as disorder, this degeneracy may be lifted, resulting in a doublet. Because the 118, 129, and 147 cm^{-1} vibrations are closely spaced, it is difficult to make definite assignments. Although the E_g Raman mode is observed at $\approx$122 cm^{-1},[24] which is close to the observed modes, it is quite weak and is normally not observed. Because this mode would have to be activated by disorder to become infrared active, it would likely be much weaker than any of the observed vibrations. The mode at 78 cm^{-1} falls well below the estimated phonon frequencies, and does not readily suggest an assignment. However, because this mode is visible in $\sigma_1(\omega)$ above T_c at 30 K, it is not related to the superconductivity in this material. There is also a possibility that this mode (and perhaps others) may be a low-lying electronic transition due to crystal-field excitations.[28] A similar quartet of lines has also been observed at slightly higher frequency ($\approx$150$-$170 cm^{-1} region) in lightly doped $La_{2-x}Sr_xCuO_4$,[36] where it was proposed that the observed tilting of the CuO_6 octahedra[39] at low temperature was responsible for the quartet. Thus, while doping-induced disorder may be responsible for the splitting of the low-frequency modes, it may also be the case that a similar distortion of the CuO_2 planes may lead to a splitting of the E_u mode. While the oscillator strengths of these modes are difficult to determine because of the rapidly changing backgrounds above and below T_c (as may be seen in Fig. 3), they appear to be much larger than in the lightly doped $La_{2-x}Sr_xCuO_4$ material. If this structure is due to phonons, then these large oscillator strengths may be an indication of electron-phonon coupling.

B. Electronic properties

The optical conductivity in the normal state in Fig. 2 shows a rapidly narrowing Drude-like component. The temperature-dependent damping $\Gamma_0=\Gamma(\omega\rightarrow 0)$ shown in Fig. 6 indicates that at low temperature Γ_0 saturates to a value of $\approx$100 cm^{-1}. An estimate of the Fermi velocity in the CuO_2 planes of $v_F\approx 2.2\times 10^7$ cm/s may be obtained from band-structure calculations,[40] which yields a mean free path ($l=v_F/\Gamma_0$) of $\approx$750 Å at 30 K. This large value for the mean free path at low temperature indicates that the doping-induced disorder in the Nd(Ce) layers does not lead to strong scattering in the CuO_2 planes.

The observation that there is relatively little scattering in the CuO_2 planes is consistent with the description of a ''clean-limit'' system [$\xi_0<l<\lambda_{ab}$, where the coherence length is $\xi_0\approx 70-80$ Å (Ref. 9)]. In the BCS theory[14] the determination of the penetration depth at $T=0$ is described by $\lambda_{ab}\approx\lambda_L(1+\xi_0/l)$; the local clean-limit approximation ($\xi_0/l\ll 1$) implies that $\lambda_{ab}\approx\lambda_L$, thus the measured penetration depth is essentially the London penetration depth.

In a clean-limit system, most of the normal-state carriers are expected to collapse into the δ function below T_c. However, estimates of the strength of the condensate indicate that only $\approx$40% of the normal-state carriers have condensed at $T_c/2$. In a variation of the two-component model, it has been suggested that the carriers responsible for much of the mid-infrared component may be centered at very low frequency ($\omega\rightarrow 0$);[41] essentially creating another distinct ''free-carrier'' component. In this picture, there are now two separate types of carriers in the normal state; (i) a narrow Drude component ($\Gamma\approx$100 cm^{-1} at 30 K), all of which collapses into the δ function below T_c, and (ii) heavily damped carriers ($\Gamma>$1000 cm^{-1}) whose properties do not change below T_c. If ω_{pD} is the plasma frequency of the Drude carriers, and ω_{pO} is the plasma frequency of the overdamped carriers, then it must be true that $\omega_{pD}^2+\omega_{pO}^2=\omega_p^2$, where ω_p is the plasma frequency of both types of carriers, as determined by optical conductivity sum rules. Thus, the requirement that $\omega_{pD}\approx\omega_{pS}(\propto\delta^{1/2})$ satisfies the clean-limit condition. This estimate works reasonably well, as $\omega_{pD}\approx$10 000 cm^{-1} for the Drude component, and the resulting value for $\omega_{pO}\approx$12 500 cm^{-1} can fit the 30 K conductivity out to $\approx$1000 cm^{-1} nearly as well as the midinfrared excitations, which are shown in Fig. 2.

While the hope-doped cuprates, such as $YBa_2Cu_3O_{6+x}$, all show a general depression of the conductivity in the far infrared for $T\ll T_c$, at low frequency there is a considerable amount of residual conductivity[42] (absorption[43]). This residual conductivity is usually taken as one of the indications that the energy gap is not a BCS-like gap. While there is a substantial reduction of the low-frequency conductivity below T_c in Fig. 3, and the conductivity appears to be decreasing down to the lowest measured frequency, there is a rather large error associated with the low-frequency conductivity due to the high value of the reflectance. Thus, the uncertain nature of the conductivity in this region makes it difficult to draw conclusions about the nature of the gap, BCS or otherwise.

In ordinary metals where there is strong coupling between electrons and phonons, the conduction electrons may be scattered inelastically by phonons. In the normal state, this process has a definite threshold at the frequency of the phonon Ω_0 (at $T=0$). As a result, a sideband starting at Ω_0 appears in the conductivity. The spectral weight of this feature (normalized to the free-carrier contribution) is equal to the electron-phonon coupling constant λ_{tr},[44] appropriate for transport but thought to be closely related to the λ in the Eliashberg strong-coupling theory of superconductivity.[45]

Below T_c, the development of an isotropic gap of 2Δ at the Fermi surface requires an energy of 2Δ to break the quasiparticle pairs; as a result the threshold for quasiparticle scattering now shifts to a higher frequency $\Omega_0+2\Delta$. The mechanism is referred to as the Holstein emission process.[46] In conventional strong-coupling metals, such as lead, a Holstein sideband due to electron-phonon coupling has been observed in the superconducting state.[47]

To achieve high T_c's in strongly coupled metals requires $\lambda \gtrsim 1$,[48,49] and estimates of the electron-phonon spectral density in cuprate systems yield similar values for λ.[50] Thus, it was expected that the Holstein structure would be strong in this material. However, as Fig. 3 and the phonon parameters listed in Table I indicate, for $T \gtrsim T_c$ and $T \ll T_c$ there are *no* anomalies, as the changes in the phonon parameters (in particular the frequencies) are very small and no new spectral features are observed. This implies that the phonons are almost totally decoupled from the electronic continuum, and that λ is very small ($\lambda \ll 1$).

An estimate of strength of the electron-phonon coupling constant for the free carriers may also be calculated from the frequency-dependent scattering rate[51]

$$\hbar/\tau \approx 2\pi\lambda_{tr}k_B T, \quad (T \geqslant \theta_D). \tag{6}$$

(It is important to note that this is a high-temperature expression.) An examination of the scattering rate in Fig. 6 in the linear region ($T \gtrsim 150$ K) yields $\lambda_{tr}=0.59\pm0.1$, which places this material in the weak-coupling limit; the value for λ_{tr} will scale depending upon the choice of ω_p. This value for λ_{tr} is larger than a previously measured value ($\lambda_{tr}=0.15\pm0.01$) for $Nd_{1.85}Ce_{0.15}CuO_4$,[36] but is similar to results obtained for hole-doped cuprates.[15] The generally small value for λ_{tr} for the superconducting carriers does not preclude the possibility of strong electron-phonon coupling with those normal-state carriers that have not condensed.[41] Because these carriers are overdamped, a Holstein sideband in the normal state would be broadened,[52] and below T_c no additional structure would be expected, as these carriers do not condense. The likelihood that the Holstein sidebands are absent and the small value for λ_{tr} suggests that the superconductivity in this material is not phonon mediated. However, by itself this is not evidence of a non-BCS mechanism; the BCS mechanism simply requires an attractive interaction.

A recent study of $Ba_{0.6}K_{0.4}BiO_3$ ($T_c \approx 30$ K) (Ref. 54) concluded that despite reports of a large value for the electron-phonon coupling constant $\lambda \approx 1$, and behavior which demonstrated an order parameter with an *s*-wave symmetry,[53] the electron-phonon coupling in $Ba_{0.6}K_{0.4}BiO_3$ must necessarily be small, $\lambda \approx 0.2$. This led to the conclusion that $Ba_{1-x}K_xBiO_3$ was an *s*-wave superconductor that is not driven by the electron-phonon interaction.

It has been observed that in many underdoped and optimally doped cuprates, the strength of the condensate δ varies monotonically with T_c.[55] This relationship is depicted in Fig. 8 for several cuprates ($La_{2-x}Sr_xCuO_4$, $YBa_2Cu_3O_{6+x}$, and $Bi_2Sr_2Ca_2Cu_3O_{10}$); the dashed line upon which these points lie is generally referred to as the Uemura line. A point has also been included for a superconducting oxide that is not based on CuO_2 planes and that is also believed to be an electron-doped material,

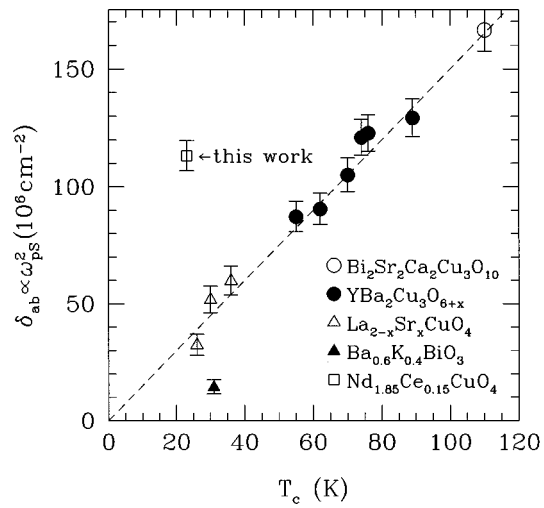

FIG. 8. The strength of the condensate $\delta \propto \omega_{pS}^2$ as a function of T_c for $La_{2-x}Sr_xCuO_4$ (open triangles), $YBa_2Cu_3O_{6+x}$ (filled circles), $Bi_2Sr_2Ca_2Cu_3O_{10}$ (open circle) (Ref. 54), $Ba_{0.6}K_{0.4}BiO_3$ (solid triangle, Ref. 40), and $Nd_{1.85}Ce_{0.15}CuO_4$ (open square, this work). The dashed line is the universal Uemura line. While the majority of the underdoped and optimally doped cuprates fall on the Uemura line, and the bismuthate just below, the value for $Nd_{1.85}Ce_{0.15}CuO_4$ obtained in this work places it well outside this linear relationship. This suggests that the nature of the superconductivity in $Nd_{1.85}Ce_{0.15}CuO_4$ is different than in other hole-doped cuprates.

$Ba_{0.6}K_{0.4}BiO_3$;[41] this material falls somewhat below the Uemura line. However, the value of the condensate ($\omega_{pS}=10\,640$ cm^{-1}) obtained for the cuprate $Nd_{1.85}Ce_{0.15}CuO_4$ lies nowhere near the other points. This is surprising in view of the fact that this material is nearly optimally doped and that other ''disordered alloy'' systems such as $La_{2-x}Sr_xCuO_4$, in the underdoped and optimally doped regions, are well described by the Uemura relationship. It is unlikely that this behavior is due to the material being overdoped, as the condensate in materials which lack chains is observed to *decrease* in the overdoped regime.[56] This suggests that the superconductivity in this material is fundamentally different that other hole-doped cuprate superconductors.

V. CONCLUSIONS

The reflectance of $Nd_{1.85}Ce_{0.15}CuO_4$ has been measured over a wide frequency range above and below T_c, and the optical properties determined. In addition to the expected four infrared-active E_u modes, a number of *c*-axis infrared and Raman modes are activated by doping-induced disorder, and are observed at low temperature in the *ab* plane. Several of the activated features have very large oscillator strengths, which may be an indication of electron-phonon coupling. Strong electron-phonon coupling may suggest a distortion of the Nd(Ce)O and CuO_2 layers. There is also the possibility that some of these features may be due to low-lying electronic transitions due to crystal-field excitations.

In the normal state the optical conductivity consists of a narrow Drude-like feature that narrows rapidly with decreasing temperature, and a midinfrared component that can be described by overdamped oscillators; there is some evidence

that part of the midinfrared band may be due to very low-frequency excitations ($\omega \rightarrow 0$), which may essentially behave like a second ''free-carrier'' component. Below T_c, only the Drude carriers collapse into the δ function. The plasma frequency of the condensate is $\omega_{pS} \approx 10\,000 \pm 600$ cm^{-1}, giving a (London) penetration depth of $\lambda_{ab} \approx 1600 \pm 100$ Å at 10 K. From transport measurements, $\lambda_{tr} < 0.5$; as well, no Holstein sidebands are observed below T_c. This indicates that the carriers that participate in superconductivity are only weakly coupled to the phonons, suggesting that if the superconductivity in this material can be described by the BCS model, then the pairing is not to due to the electron-phonon mechanism. While optical techniques cannot unambiguously determine the symmetry of the superconducting energy gap, the strength of the condensate in $Nd_{1.85}Ce_{0.15}CuO_4$ is much larger than in other cuprate materials with similar T_c's, indicating that the superconductivity in this material is different than in other cuprate superconductors.

ACKNOWLEDGMENTS

The authors would like to acknowledge many useful discussions with D. N. Basov, D. A. Bonn, A. V. Puchkov, and T. Timusk. We are grateful to A. W. McConnell for assistance in the laboratory. This work was supported by the Natural Sciences and Engineering Research Council of Canada, the Linville Institute, and Simon Fraser University. Work at Maryland is supported by the NSF under Contract No. DMR-9510475.

*Present address: Department of Physics, Brookhaven National Laboratory, Upton, NY 11973-5000. Electronic address: homes@solids.phy.bnl.gov

[1] Y. Tokura, H. Takagi, and S. Uchida, Nature (London) **377**, 345 (1989); H. Takagi, S. Uchida, and Y. Tokura, Phys. Rev. Lett. **62**, 1197 (1989).

[2] W. Jiang, S N. Mao, X. X. Xi, X. Jiang, J. L. Peng, T. Venkatesan, C. J. Lobb, and R. L. Greene, Phys. Rev. Lett. **73**, 1291 (1994).

[3] H. Müller-Buschbaum and W. Wollschläger, Z. Anorg. Chem. 414, 76 (1975).

[4] B.-H. O and J. T. Markert, Phys. Rev. B **47**, 8373 (1993).

[5] W. N. Hardy, D. A. Bonn, D. C. Morgan, R. Liang, and K. Zhang, Phys. Rev. Lett. **70**, 3999 (1993).

[6] Z.-X. Shen, D. S. Dessau, B. O. Wells, D. M. King, W. E. Spicer, A. J. Arko, D. Marshall, L. W. Lombardo, A. Kapitulnik, P. Dickinson, S. Doniach, J. DiCarlo, A. G. Loeser, and C. H. Park, Phys. Rev. Lett. **70**, 1553 (1993).

[7] D.-H. Wu, J. Mao, S. N. Mao, J. L. Peng, X. X. Xi, T. Venkatesan, R. L. Greene, and S. M. Anlage, Phys. Rev. Lett. **70**, 85 (1993).

[8] A. Andreone, A. Cassinese, A. DiChiara, R. Vaglio, A. Gupta, and E. Sarnelli, Phys. Rev. B **49**, 6392 (1994).

[9] S. M. Anlage, D.-H. Wu, J. Mao, S. N. Mao, X. X. Xi, T. Venkatesan, J. L. Peng, and R. L. Greene, Phys. Rev. B **50**, 523 (1994).

[10] Q. Huang, J. F. Zasadzinksi, N. Tralshawala, K. E. Gray, D. G. Hinks, J. L. Peng, and R. L. Greene, Nature (London) **347**, 369 (1990).

[11] S. C. Sanders, O. B. Hyun, and D. K. Finnemore, Phys. Rev. B **42**, 8035 (1990).

[12] R. Calemczuk, A. F. Khoder, C. Marcenta, E. Bonjour, C. Martin, and J. Y. Henry, Physica B **194**, 1493 (1994).

[13] E.-J. Choi, K. P. Stewart, S. K. Kaplan, H. D. Drew, S. N. Mao, and T. Venkatessan, Phys. Rev. B **53**, R8859 (1996).

[14] M. Tinkham, in *Introduction to Superconductivity* (McGraw-Hill, New York, 1975), pp. 57–71.

[15] D. B. Tanner and T. Timusk, in *Physical Properties of High-Temperature Superconductors III*, edited by D. M. Ginsberg (World Scientific, Singapore, 1992).

[16] S. H. Wang, Q. Song, B. P. Clayman, J. L. Peng, L. Zhang, and R. N. Shelton, Phys. Rev. Lett. **64**, 1067 (1990).

[17] A. P. Litvinchuk, C. Thomsen, P. Murugaraj, E. T. Heyen, and M. Cardona, Phys. Rev. B **43**, 13 060 (1991).

[18] R. A. Hughes, Y. Lu, T. Timusk, and J. S. Preston, Phys. Rev. B **47**, 985 (1993).

[19] Y. Watanabe, Z. Z. Wang, S. A. Lyon, N. P. Ong, D. C. Tsui, J. M. Tarascon, and E. Wang, Solid State Commun. **74**, 757 (1990).

[20] J.-G. Zhang, X.-X. Bi, E. McRae, P. C. Eklund, B. S. Sales and M. Mostoller, Phys. Rev. B **43**, 5389 (1991).

[21] S. Uchida, T. Ido, H. Takagi, T. Arima, Y. Tokura, and S. Tajima, Phys. Rev. B **43**, 7942 (1991).

[22] S. Lupi, P. Calvani, M. Capizzi, P. Maselli, W. Sadowski, and E. Walker, Phys. Rev. B **45**, 12 470 (1992).

[23] M. K. Crawford, G. Burns, G. V. Chandrashekhar, F. H. Dacol, W. E. Farneth, E. M. McCarron III, and R. J. Smalley, Phys. Rev. B **41**, 8933 (1990).

[24] E. T. Heyen, G. Kliche, W. Kress, W. König, M. Cardona, E. Rampf, J. Prade, U. Schröder, A. D. Kulkarni, F. W. de Wette, S. Piñol, D. McK. Paul, E. Morán, and M. A. Alario-Franco, Solid State Commun. **74**, 1299 (1990).

[25] S. Sugai, T. Kobayashi, and J. Akimitsu, Phys. Rev. B **40**, 2686 (1989).

[26] I. Tomeno, M. Yoshida, K. Ikeda, K. Tai, K. Takamuku, N. Koshizuka, S. Tanaka, K. Oka, and H. Unoki, Phys. Rev. B **43**, 3009 (1991).

[27] B. Stadlober, G. Krug, R. Nemetschek, R. Hackl, J. L. Cobb, and J. T. Markert, Phys. Rev. Lett. **74**, 4911 (1995).

[28] S. Jandl, P. Dufour, T. Strach, T. Ruf, M. Cardona, V. Nekvasil, C. Chen, B. M. Wanklyn, and S. Piñol, Phys. Rev. B **53**, 8632 (1996).

[29] J. L. Peng, Z. Y. Li, and R. L. Greene, Physica C **177**, 79 (1991).

[30] C. C. Homes, M. Reedyk, D. A. Crandles, and T. Timusk, Appl. Opt. **32**, 2976 (1993).

[31] For a fit to $\sigma_1(\omega)$ at 30 K the Drude component in Fig. 2 consists of $\omega_{pD} = 11\,100$ cm^{-1} and $\Gamma_D = 48$ cm^{-1}, while the midinfrared band has been generated using four (arbitrary) Lorentzian oscillators; (i) $\omega_1 = 130$, $\gamma_1 = 160$, $\omega_{p1} = 5500$, (ii) $\omega_2 = 240$, $\gamma_2 = 550$, $\omega_{p2} = 7000$, (iii) $\omega_3 = 800$, $\gamma_3 = 2050$, $\omega_{p3} = 8000$ and, (iv) $\omega_4 = 2800$, $\gamma_4 = 4600$, $\omega_{p4} = 14\,000$. (All units are in cm^{-1}.)

[32] A. Puchkov, D. N. Basov, and T. Timusk, J. Phys. Condens. Matter **8**, 10 049 (1996).

[33] S. J. Hagen, J.-L. Peng, Z. Y. Li, and R. L. Greene, Phys. Rev. B **43**, 13 606 (1991).

[34] J. F. Scott, Phys. Rev. B **4**, 1360 (1971).

[35] S. Tajima, T. Ido, S. Ishibashi, T. Itoh, H. Eisaki, Y. Mizuo, T.

Arima, H. Takagi, and S. Uchida, Phys. Rev. B **43**, 10 496 (1991).
[36] D. B. Tanner, Y.-D. Yoon, A. Zibold, H. L. Liu, M. A. Quijada, S. W. Moore, and J. M. Graybeal, Proc. SPIE **2696**, 13 (1996).
[37] M. J. Rice, Phys. Rev. Lett. **37**, 36 (1976).
[38] M. J. Rice, L. Pietronero, and P. Bruesch, Solid State Commun. **21**, 757 (1977).
[39] B. Büchner, M. Breuer, A. Freimuth, and A. P. Kampf, Phys. Rev. Lett. **73**, 1841 (1994).
[40] P. B. Allen, W. B. Pickett, and H. Krakauer, Phys. Rev. B **37**, 7482 (1988).
[41] A. V. Puchkov, T. Timusk, W. D. Mosley, and R. N. Shelton, Phys. Rev. B **50**, 4144 (1994).
[42] D. N. Basov, R. Liang, D. A. Bonn, W. N. Hardy, B. Dabrowski, M. Quijada, D. B. Tanner, J. P. Rice, D. M. Ginsberg, and T. Timusk, Phys. Rev. Lett. **74**, 598 (1995).
[43] T. Pham, H. D. Drew, S. H. Moseley, and J. Z. Liu, Phys. Rev. B **41**, 11 681 (1990); T. Pham, M. W. Lee, H. D. Drew, U. Welp, and Y. Fang, Phys. Rev. B **44**, 5377 (1991).
[44] P. B. Allen, Phys. Rev. B **3**, 305 (1971).
[45] G. M. Eliashberg, Sov. Phys. JETP 11, 696 (1960).
[46] T. Holstein, Ann. Phys. (N.Y.) **29**, 410 (1964).
[47] R. R. Joyce and P. L. Richards, Phys. Rev. Lett. **24**, 1007 (1970).
[48] W. L. McMillan, Phys. Rev. **167**, 331 (1968).
[49] P. B. Allen and R. C. Dynes, Phys. Rev. B **12**, 905 (1975).
[50] J. Orenstein, G. A. Thomas, A. J. Millis, S. L. Cooper, D. H. Rapkine, T. Timusk, L. F. Schneemeyer, and J. V. Waszczak, Phys. Rev. B **42**, 6342 (1990).
[51] P. B. Allen, T. P. Beaulac, F. S. Khan, W. H. Butler, F. J. Pinski, and J. C. Swihart, Phys. Rev. B **34**, 4331 (1986).
[52] D. Miller, P. L. Richards, E. J. Nicol, E. S. Hellman, E. H. Hartford Jr., C. E. Platt, R. A. Schweinfurth, D. J. Van Harlington, and J. Amano, J. Phys. Chem. Solids **54**, 1323 (1994).
[53] F. J. Dunmore, H. D. Drew, E. J. Nicol, E. S. Hellman, and E. H. Hartford, Phys. Rev. B **50**, 643 (1994).
[54] F. Marsiglio, J. P. Carbotte, A. Puchkov, and T. Timusk, Phys. Rev. B **53**, 9433 (1996).
[55] Y. J. Uemura, L. P. Le, G. M. Luke, B. J. Sternlieb, W. D. Wu, J. H. Brewer, T. M. Riseman, C. L. Seaman, M. B. Maple, M. Ishikawa, D. G. Hinks, J. D. Jorgensen, G. Saito, and H. Yamochi, Phys. Rev. Lett. **66**, 2665 (1991).
[56] J. L. Tallon, C. Bernhard, U. Binninger, A. Hofer, G. V. M. Williams, E. J. Ansaldo, J. I. Budnick, and Ch. Niedermayer, Phys. Rev. Lett. **74**, 1008 (1995).